Diffusion Monte Carlo: A pathway towards an accurate theoretical description of manganese oxides

Kayahan Saritas,[1,*] Jaron T. Krogel,[1,†] P. R. C. Kent,[2,‡] and Fernando A. Reboredo[1,§]

[1]*Materials Science and Technology Division, Oak Ridge National Laboratory, Oak Ridge, Tennessee 37831, USA*

[2]*Center for Nanophase Materials Sciences and Computational Science and Engineering Division, Oak Ridge National Laboratory, Oak Ridge, Tennessee 37831, USA*

(Received 5 August 2017; revised manuscript received 22 May 2018; published 14 August 2018)

We present diffusion Monte Carlo (DMC) results for equation of state and quasiparticle gaps of manganese binary oxides MnO and MnO_2 and the ternary oxide $LaMnO_3$. Owing to the limited approximations made and the direct treatment of electronic correlations, our DMC-based study correctly describes structural properties such as the lattice constant, bulk moduli, and cohesive energies. It correctly predicts the ground-state phase of these oxides, which have different valences. Our study demonstrates the capability of DMC methods to predict the structural properties of highly correlated systems, which have been identified as suitable candidates for many applications ranging from catalysis to electronic devices. Our study also serves as a benchmark for both the manganese pseudopotential and other methodological choices to be used in calculations of similar oxides.

DOI: 10.1103/PhysRevMaterials.2.085801

I. INTRODUCTION

Transition metal oxides (TMOs) possess a variety of structures and exhibit a multitude of collective effects such as metal-insulator transitions; ferro-, ferri-, and antiferromagnetism; ferroelectricity; superconductivity; colossal magnetoresistance; etc. [1–11]. The unusual electronic properties of TMOs are closely related to the strongly correlated nature of the *d*-orbital electrons. In TMOs, the localized character of the partially filled *d* states and the multiplicity of their valence lead to the competition of several physical interactions (spin, charge, and lattice). The concurrence of strong lattice-electron, spin-electron, and spin-orbit couplings causes fascinating phenomena, including metal-insulator transitions [1–3], superconductivity [4], colossal magnetoresistance [5–7], and multiferroicity [7]. Their band gaps span from the infrared to the ultraviolet [8], while their surface chemical reactivity ranges from active to inert [9,10].

To understand and predict the structural, electronic, and magnetic properties of these oxides using theoretical methods, it is necessary to have a reliable description of the electronic structure. Because of the strong electron correlation, it is very challenging to model these materials from first principles. Conventional methods based on density functional theory [12–14] (DFT) approximations are seldom accurate enough to account for the electronic structure of materials with localized *d*-orbitals and frequently lead to unrealistic results. In particular, for transition-metal oxides, the electronic self-interaction error [15] propagates with the treatment of the Coulomb interaction [16–29].

Since transition metals are multivalent in nature, each valence state can result in different oxide crystal structures with a qualitative different crystalline field around the transition metal atom. The identification of the correct lowest energy lattice structure is a strong validation of the accuracy of the theoretical approximations used to calculate the electronic structure. In manganese oxides, it is well established experimentally that the rock salt (RS) phase is the most stable form of MnO. However, some methods and approximations [30,31] predict the zinc blende (ZB) structure to be lower in energy. The magnetic ground-state configuration also depends on the approximation used [32,33].

Rapid advancements in the development of electronic-structure methods such as quantum Monte Carlo (QMC) [34–37] and increasing computational resources have provided a viable alternative theoretical approach for these complex systems. Because of the few fundamental approximations made and the direct treatment of electron correlation, QMC methods—such as fixed-node diffusion Monte Carlo (FN-DMC)—are among the most accurate electronic structure methods available [38]. The number of published reports using DMC in elemental solids, semiconductors, metals, oxides, and transition metal-oxides [16–29,39–45] is still very small compared with similar calculations using DFT approximations even though DMC methods already show systematic improvements compared with DFT methods. Nevertheless, since this type of calculation is not routine, the parameters required to obtain accurate results with high-performance-computer resources, as well as the validity of the pseudopotentials and other fundamental approximations of the approach, need to be established for every material family before more demanding calculations are attempted.

In this contribution, we assess the accuracy of the DMC method in predicting the structural and electronic properties of some manganese-based binary oxides (MnO and MnO_2) and the ternary oxide $LaMnO_3$. The DMC calculated cohesive energies and structural parameters (equilibrium lattice constants and bulk modulus) are within the uncertainty of the available experiments. Our study demonstrates the capability of DMC

*saritask@ornl.gov
†krogeljt@ornl.gov
‡kentpr@ornl.gov
§reboredofa@ornl.gov

methods to predict the structural properties of highly correlated systems. We also find that for these manganese compounds, the structural properties such as cohesive energy, equilibrium lattice constants, and bulk modulus are not modified by the fundamental approximations in the theoretical approach. For detailed discussion regarding the approximations involved, see Secs. IIC– IIF.

The rest of the paper is organized as follows: in Sec. II, we give a brief overview of the computational details and the DMC method. In Sec. III, we present and discuss our main results: DMC-calculated structural properties of MnO, MnO_2, and $LaMnO_3$ compared with experiments and various computational approaches. We focus on (1) the bulk properties: cohesive energies and equation of states and (2) quasiparticle gaps. In Sec. IV, we compare the performance of exchange-correlation functionals with DMC for various manganese-based oxides. Finally, we summarize our findings in Sec. IV.

II. COMPUTATIONAL DETAILS

A. Diffusion Monte Carlo

QMC methods use statistical sampling to evaluate many-body wave functions. In these methods the total energies are directly evaluated from the first-principles many-body Schrödinger equation, which greatly reduces the extent of necessary approximations. In the present work, to assess the properties of manganese-based oxides we applied the FN-DMC method as implemented in the QMCPACK code [36]. The entire study was managed, monitored, and analyzed using the modular workflow automation system Nexus [46]. Since the details of the DMC approach are already available in the literature [38,47–50], here we provide only a brief overview.

FN-DMC finds the lowest energy of all the wave functions that share the nodes (or the phases) of an input trial wave function. This constraint forces the wave function to remain antisymmetric (fermionic). Within the fixed-node approximation, the DMC algorithm projects out all the excited state components of the wave function except the ground state. To define the nodal surfaces, a reasonable and commonly chosen starting point for the trial wave function is to use orbitals from DFT calculations or other mean field approaches. The ground-state energy is only exact if the exact nodes are provided. The nodal error is a positive contribution to the exact ground state energy. The finite-size (FS) errors also affect the accuracy of DMC results. Two potential sources for these errors are (1) single-particle errors and (2) the artificial periodicity of the exchange-correlation hole. The first error arises from the discrete sampling of the Brillouin zone, which can be minimized by using twist-averaged boundary conditions [51]. The second error can be minimized by increasing the size of the supercells. To minimize the FS errors, in the present work, the DMC calculations were performed using twist-averaged boundary conditions [51] on 64-, 48-, and 40- atom supercells for MnO, MnO_2, and $LaMnO_3$, respectively.

B. Trial wave-function construction

The Slater-Jastrow form with the single particle orbitals obtained from DFT was used as trial wave functions. The Slater determinants [50,52,53] were constructed with DFT orbitals. Electron correlations were introduced to the trial wave function via a correlating Jastrow factor [54]:

$$\psi(R) = e^{-J(R)} D_\uparrow(R) D_\downarrow(R), \tag{1}$$

where the Slater determinants $D_\uparrow(R)$ and $D_\downarrow(R)$ correspond to spin-up and spin-down subspaces, respectively. Conventionally, the Jastrow factor $J(R)$ is the sum of the contributions from electron-ion, electron-electron, and electron-electron-ion correlation terms. These terms are known as one-body ($e^{-J_1(R)}$), two-body ($e^{-J_2(R)}$), and three-body ($e^{-J_3(R)}$) Jastrow terms, respectively. To accelerate the generation of results to the desired statistical accuracy, we optimize parameters in the Jastrow factors with energy and variance minimization within variational Monte Carlo [55].

In this work, we used trial wave functions of a single-determinant Slater-Jastrow form with one- and two-body Jastrow factors because the increasing computational cost required for evaluation of the three-body Jastrow did not result in a significant reduction of the error bar.

For the DMC calculations of oxides, monoatomic solids (lanthanum and manganese), and oxygen molecules, the single-particle orbitals used in the trial wave function were generated with the local density approximation (LDA) [15] as implemented in the Quantum ESPRESSO (QE) package [56]. Convergence tests of plane-wave cutoff energies (E_{cut}), k-point meshes, and smearing parameters were performed for all the compounds considered in the present work. A strict convergence criterion was used: ± 1.0 mRy per formula unit in the ground-state energy. In the case of MnO, 8-atom cells were used for both RS and ZB in conjunction with an $8\times8\times8$ Monkhorst-Pack sampling of k-points in the Brillouin zone. While for MnO_2 and $LaMnO_3$, 6-atom and 10-atom cells were used. The QMC calculations were performed in larger supercells. The wave functions were constructed using translational symmetry from the wave functions of smaller cells to save memory. For DMC calculations, the wave function was unfolded to 64-, 48-, and 40-atom supercells for MnO, MnO_2, and $LaMnO_3$, respectively.

QE was used solely as a source of orbitals for QMC. DFT results reported in the present work were calculated using the Vienna *ab initio* software package (VASP) [57,58].

C. Fixed-node error

Because the approximations in DMC can be systematically improved, it has produced results with exceptional accuracy [17,21,59]. However, as mentioned previously, DMC requires the following approximations. In DMC methods, the fixed-node approximation is introduced to maintain the antisymmetry of the wave function and to overcome the fermion sign problem (the determination of the node, where the wave function changes sign). The fixed-node approximation prevents walker moves that cross fermion nodes and change the sign of the trial wave function. The fixed-node approximation in DMC gives exact results if the trial nodal surface is exact. Although the fixed-node error is small (typically, a few percent of the correlation energy), the error can still be too large for some applications, particularly in important cases of computating very small energy differences. In the present work, we have explored the nodal surfaces arising from the Hubbard-corrected LDA

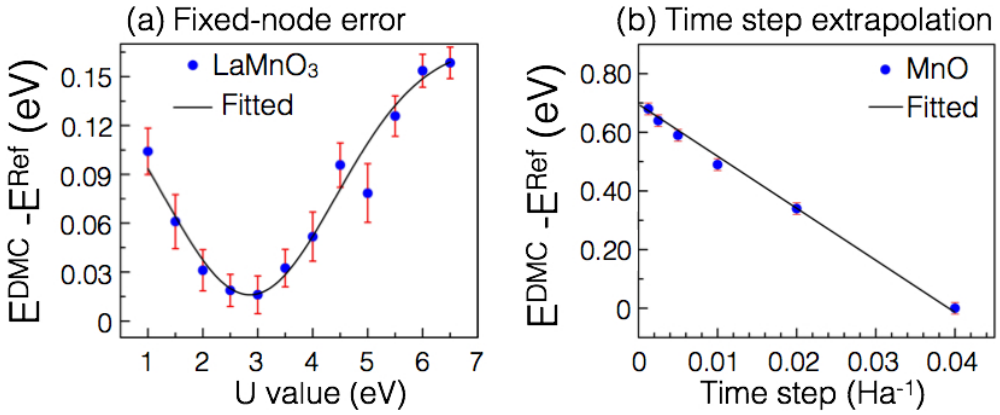

FIG. 1. (a) Minimization of fixed-node error. Calculated DMC energies for $LaMnO_3$ (40-atom supercell) as a function of Hubbard parameter U. (b) Time-step extrapolation. DMC energies of the RS phase of MnO as a function of time step. Reference energies (E^{Ref}) for panels (a) and (b) are −5015.82 eV and −3273.00 eV, respectively.

functionals to perform a simple one-parameter optimization of the nodal surface. As a representative case in Fig. 1, we show the DMC energy as a function of Hubbard parameter U for $LaMnO_3$. Our DMC calculations found that U values of 3.5, 3.5, and 3 eV minimize the DMC energies for MnO, MnO_2, and $LaMnO_3$, respectively. The subsequent calculations were performed using these U values.

D. Pseudopotential generation

Pseudopotentials (PPs) are the backbone of DMC simulations, and the accuracy of the DMC results significantly depends on the availability of high-quality PPs. At present, generation of PPs within DMC is not practical. Before use with DMC, PPs must be carefully tested with other theories (such as Hartree-Fock or DFT). In the present work, we used norm-conserving PPs for the oxygen, manganese, and lanthanum atoms, which are generated with OPIUM. The O-PP is based on a He-core PP. All PPs are tested and used for DMC studies of dimers and solids [17,21,59]. Our PPs have been shown to present Jastrow sensitivities comparable or better to previously developed Hartree Fock PPs appropriate for Gaussian basis set calculations [60]. The hard PPs used in the present work require a high plane-wave cutoff energy. Therefore, for MnO, MnO_2, and $LaMnO_3$, a plane-wave energy cutoff was set to 350, 350, and 300 Ry, respectively. To treat the nonlocal part of the PPs within DMC and avoid the numerical instabilities of the locality approximation, the T-moves [61] scheme was used.

E. Time-step error

In principle, DMC provides the fixed-node solution of the imaginary time-dependent Schrödinger equation, where the many-body wave function is statistically sampled using a Green's function approach by propagating a set of walkers in a $3N$-dimensional space (N is the number of electrons). Since the Green's function projector obtained within the short time approximation is exact only in the limit of a vanishingly small time step ($\tau \simeq 0$), finite time steps introduce a time-step error. It is important to show that errors in the projected energy, due to the finite time step, are small. Note that the associated computational cost for the same statistical error increases as τ^{-1}.

To understand the effect of DMC time step, in Fig. 1(b) we have plotted the DMC energies (twist averaged over k-points) calculated for the rocksalt phase of MnO as a function of the DMC time step. It is evident from Fig. 1(b) that the DMC energies show a nearly linear dependence with decreasing time step. In particular, for sufficiently small time steps (smaller than 0.01 Ha^{-1}), the energy varies within ≈0.02 eV/fu of the extrapolated value. A similar trend is observed for MnO_2 and $LaMnO_3$ (not shown here). In practice, the evaluation of energies requires extrapolations to infinitesimal time step within the validity of linear extrapolation.

Although the time-step correction [Fig. 1(b)] is of the order of the statistical error for the time steps used, it is important to estimate the effect of DMC time step on the calculated properties to test the systematic cancellation of time step errors. In Figs. 2(a)–2(c), we have plotted the DMC calculated cohesive energies for MnO, MnO_2, and $LaMnO_3$ as a function of DMC time step. The DMC energies (twist averaged) for the rocksalt phase of MnO, MnO_2, and $LaMnO_3$ are calculated using a 32-, 48-, and 40-atom supercell, respectively. It is evident from Figs. 2(a)–2(c) that for all three cases the DMC cohesive energies do not show strong time-step dependence (i.e., the energy differences benefit somewhat from a cancellation of time-step errors). In the limit of zero time step, compared with experimental results, the cohesive energies differ by 0.08(4) eV/fu, 0.10(6) eV/fu, and 0.10(5) eV/fu for MnO, MnO_2, and $LaMnO_3$, respectively. Therefore a time step of 0.01 Ha^{-1} is used for the DMC calculations presented in the rest of this paper.

F. Cohesive energy and equation of state

The cohesive energy (E^{Coh}) of a solid can be determined as

$$E^{\mathrm{Coh}} = \sum E_g^i - E_s^{\mathrm{Tot}}, \tag{2}$$

where E_s^{Tot} is the total DMC or DFT energy of the solid. The respective energies of the monoatomic gas phase components are shown as E_g^i. In the case of $LaMnO_3$, E_s^{Tot} is the energy of solid $LaMnO_3$, whereas the monoatomic energies of lanthanum,

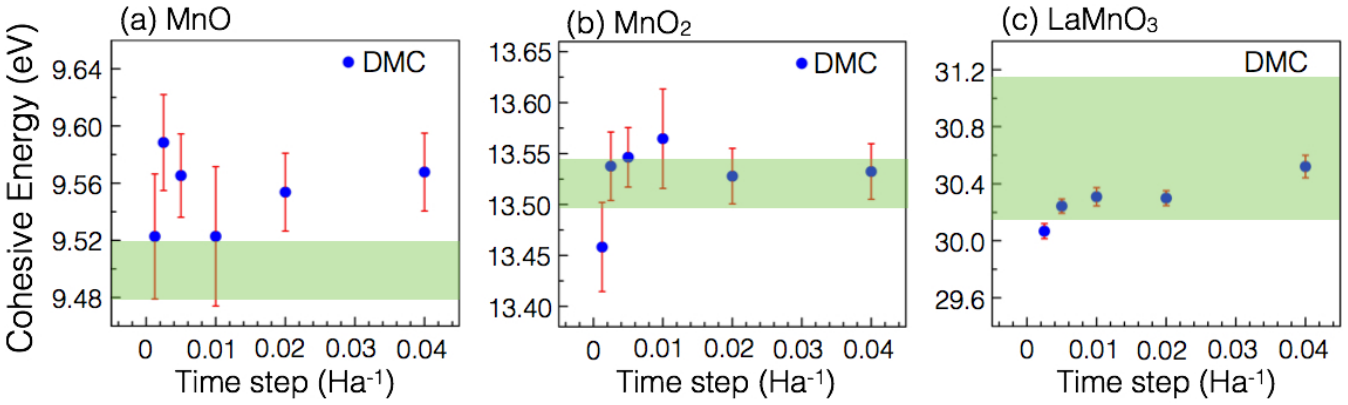

FIG. 2. Time-step dependence of the cohesive energy. DMC-calculated cohesive energies (per fu) as a function of time step for (a) RS phase of MnO, (b) β-MnO_2, and (c) $LaMnO_3$. The green regions correspond to the available experimental cohesive energies collected from MnO [73], MnO_2 [73–75], and $LaMnO_3$ [76–79]. The height of each green area represents the variations between different experimental values. The statistical uncertainties in the DMC data are shown with error bars.

manganese, and oxygen would be given as E_g^{La}, E_g^{Mn}, and E_g^{O}, respectively. We calculated the cohesive energies at 0 Kelvin and compared our results to the experimental cohesive energies in Fig. 2 [73–79]. We presented the statistical and experimental uncertainties between different results using standard deviation error bars.

Structural parameters such as equilibrium lattice constants (a), bulk modulus (B), and bulk modulus's pressure derivative (B') were calculated by fitting the Murnaghan equation of state (EOS) [80] to the total energy as a function of volume.

The Murnaghan EOS is given as

$$E_T(V) = E_T(V_0) + \frac{B_0 V}{B_0'}\left[\frac{(V_0/V)^{B_0'}}{B_0' - 1} + 1\right] - \frac{V_0 B_0}{B_0' - 1}, \quad (3)$$

where $E_T(V)$ represents the energy at volume V and B_0, B_0', and V_0 represent the bulk modulus, pressure derivative, and equilibrium volume, respectively.

The cohesive energies were calculated at the optimized geometries within each theoretical method employed (i.e., at the equilibrium volume found by each respective QMC method or DFT functional). All the DFT results reported in the figures, tables, and text were calculated using VASP [57,58] with projector augmented wave potentials.

G. Excited-state properties

We studied the quasiparticle gaps and band dispersion of MnO, MnO_2, and $LaMnO_3$ using the DMC method. The quasiparticle gap, E_g, can be calculated using the following formula:

$$E_g = E_a - \mathrm{IP}, \quad (4)$$

where E_a is the electron affinity and IP is the ionization potential. The electron affinity is defined as $E_a = E_{N+1} - E_N$, where N is the number of electrons in a charge neutral system. Similarly, the ionization potential is defined as $\mathrm{IP} = E_N - E_{N-1}$. Performing these calculations using DMC requires charged simulation cells. Therefore, DFT calculations were performed with a uniform, neutralizing background charge density to obtain trial wave functions for DMC calculations. This procedure has also been implemented in Refs. [81,82]. Charged cells introduce an error of order $1/N$, which originates in a compensating density inversely proportional to the number of electrons in the system N. Therefore, simulation cells with increasing sizes were used to extrapolate quasiparticle gaps at the infinitely large simulation cell.

To study the band dispersion, we performed excited-state DMC calculations at relevant high-symmetry k-points. We identified the high-symmetry k-points for direct and indirect transitions using DFT+U [83] calculations. Excited-state calculations were performed via promotion of an electron from valence band to conduction band. Therefore, charge neutral simulation cells were used.

III. RESULTS AND DISCUSSION

A. MnO

1. Ground-state identification

Identification of the correct ground-state structure is one of the basic results that can be expected from any computational methodology. Before investigating other structural properties, we benchmarked the adequacy of the DMC methods within the aforementioned approximations by predicting the correct ground-state phase of MnO. In the present work, DMC calculations were performed for 32-atom unit cells (for both RS and ZB) in conjunction with a 4 × 4 × 4 Monkhorst-Pack sampling of k-points in the Brillouin zone. Experimental lattice constant (4.43 Å) [66] was used for the RS phase. For the ZB phase, because of the unavailability of the experimental lattice constant, the lattice constant was obtained using the PBE0 functional (4.73 Å) [26]. In Fig. 3(a), we show the ground-state energy difference between the ZB and RS MnO phases as a function of DFT functionals (the different approximation to the exchange-correlation energy) compared with DMC results and experiment. DMC correctly predicts the stability order of the phases $E_{\mathrm{RS}} > E_{\mathrm{ZB}}$. Positive values of $(E_{\mathrm{ZB}} - E_{\mathrm{RS}})$ in Fig. 3(a) denote a more stable RS phase, which is found to be consistent with experiments and a previous DMC study [26]. For the RS-MnO, we used the AFM-II type magnetic

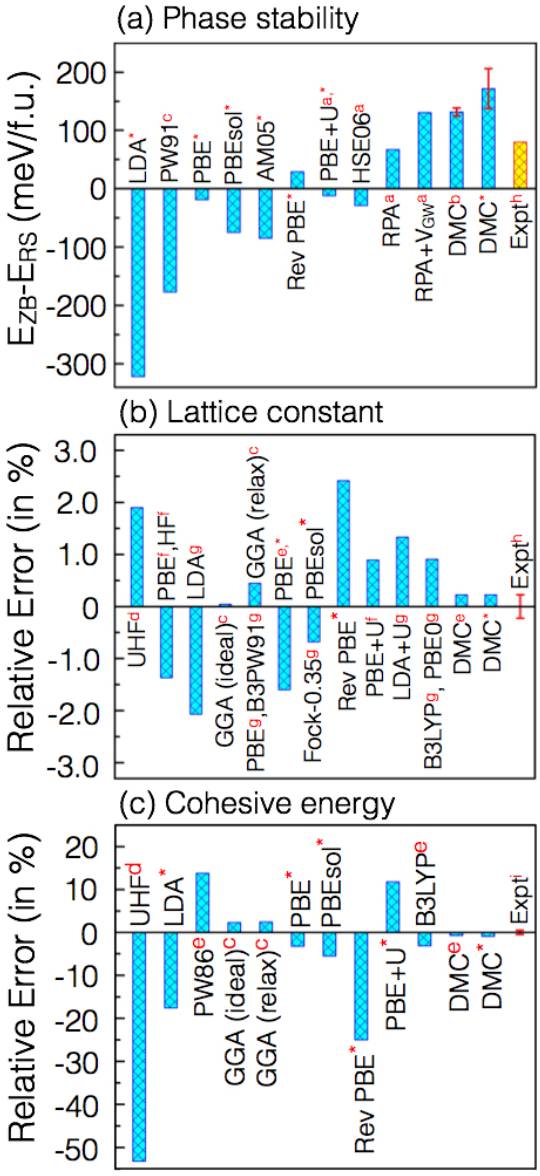

FIG. 3. An asterisk (*) denotes the results from the present work, while the other results are from *a* [30], *b* [26], *c* [31], *d* [62], *e* [63], *f* [64], *g* [65], *h* [66–70], and *i* [70–72]. (a) Comparison of the calculated and available results for phase stability (difference between total energies of ZB and RS phases) of MnO. Standard deviation error bars (red bars) show statistical uncertainties in the DMC data. Note that the experimental data drawn (in yellow) for the ground-state energy difference ($E_{ZB} - E_{RS}$) for MnO is some unknown positive quantity. (b, c) Comparison (relative error) of calculated and available theoretical and experimental results for (b) lattice constants and (c) cohesive energies of the RS phase of MnO. Statistical uncertainties in the experimental data are shown with red deviation error bars. In (b), Fock-0.35 [65] is a hybrid functional with PBE and 0.35 fraction of HF exchange.

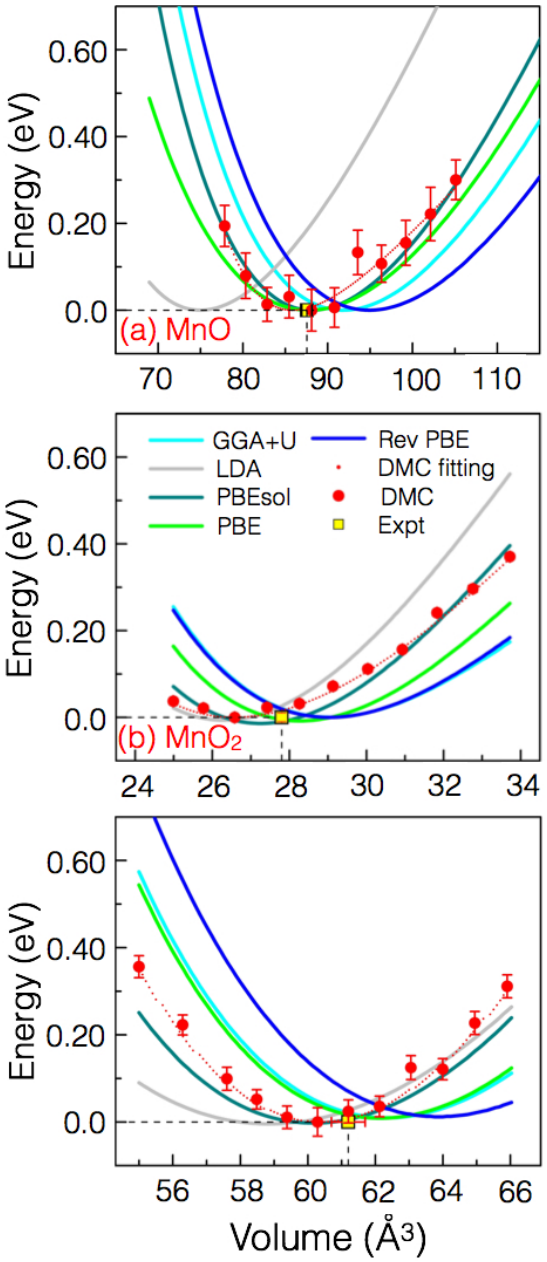

FIG. 4. EOS. DFT and DMC energies (per formula unit) versus volume (per formula unit) together with fitted Murnaghan curves for (a) RS phase of MnO, (b) β-MnO_2, and (c) $LaMnO_3$. Reference energy (E^{Ref}) is the minimum energy of the respective structure obtained from the Murnaghan fit. The statistical uncertainty in DMC energies and experimental data is also shown. In the case of MnO_2, the statistical uncertainty in DMC energies is smaller than the symbol size. The experimental equilibrium volumes for MnO [69], MnO_2 [35,91,92], and $LaMnO_3$ [76–79] are also shown for comparison. Statistical uncertainties in the experimental data is shown using standard deviation error bars.

configuration that is also found to be the magnetic ground state using neutron diffraction experiments [66,90].

2. *Structural properties*

The structural parameters—namely lattice constants (a), bulk modulus (B), and bulk modulus's pressure derivative (B')—are determined by fitting the Murnaghan EOS to the calculated data. The energy versus volume curves for the RS phase of MnO, β-MnO_2, and $LaMnO_3$ were calculated using DMC, and the various functionals of DFT are plotted in Figs. 4(a)–4(c).

First, we discuss the equilibrium lattice constant. In Fig. 3(b), we compare the relative errors (with respect to the experimental values) in lattice constants calculated within DMC, as well as using the different DFT functionals as implemented in the VASP [57,58]. Comparative analysis suggests that our DMC results agree well with the experiments and the DMC results from Mitas *et al.* [63]. The difference between both DMC results is small and within the statistical error. It is well known that generalized gradient approximation (GGA) [15] tends to overestimate the lattice parameters [93]. However, in the case of the RS phase of MnO, the GGA [31] predicted lattice constant is found to be in agreement with results from experiments and DMC calculations. For all other studied DFT functionals, the observed errors in the lattice constant range from 1 to 2% [see Fig. 3(b)].

The relative errors in the calculated cohesive energies (using DMC and various approximations using the VASP [57,58] package) for MnO in the RS phase with respect to the experimental values are shown in Fig. 3(c). Our DMC-based cohesive energy is in excellent agreement with experimental and available DMC-calculated values [63]. Note that our cohesive energies are reported at the theoretical optimum volume found within each theoretical method. Although PBE provides reasonable results for total energies across a wide range of chemical compositions, it suffers from significant electronic structure errors arising from self-interaction, as well as a tendency to disfavor the density overlap between atoms (making lattice constants larger). It is evident from Fig. 3(c) that the relative error is larger for the PBE+U than the PBE and that the deviations in cohesive energies have negative and positive signs, respectively. Although PBE+U is supposed to describe the localized nature of the electrons for oxides, the relative error of 12% for cohesive energy using PBE+U is much higher than that for PBE. However, PBE+U is more accurate than PBE for the lattice constant [see Fig. 3(b)].

In Table I, we presented our results for the optical and quasiparticle gaps of MnO compared with DFT and other DMC calculations. All DFT results reported in Table I correspond to the the band gaps that are given by the generalized Kohn-Sham eigenvalues from a band structure calculation. Table I shows our DMC results for both the optical gaps, along with the DFT results, and DMC quasiparticle gap energies (DMC_{QP}). Our PBE+U calculations yielded an indirect band gap $E_g^{K\to\Gamma}$; while the direct band gap, $E_g^{\Gamma\to\Gamma}$, was identified as $\Gamma \to \Gamma$ transition. These findings were consistent within all DFT methods we used. They are also in agreement with the LDA+U calculations of Anisimov *et al.* [83] and the GW calculations of Rodl *et al.* [94].

For MnO, and in the rest of this work, we determined the wave vectors for the direct and indirect transitions from PBE+U calculations. We performed QP calculations in DMC via a two-point extrapolation using 16- and 32-atom cells. Our DMC_{QP} results are in good agreement with the band gaps obtained from photoemission measurements [95] with E_g = 3.9(4) eV and conductivity measurements [96] with E_g = 4.0(2) eV. Whereas, our DMC indirect gap result, 3.74(19) eV, is similar to the optical absorption measurements [97] with $E_g = 3.7(1)$ eV. Our results also provide an improvement over the previously performed DMC calculations in comparison with the optical gap of 4.47(16) eV by Schiller *et al.* [26] and 4.8(2) eV by Mitas and Kolorenč [63]. For the quasiparticle gap, our results have only minimal improvement over the 4.55(26) eV calculated by Schiller *et al.* [26]. The difference in our DMC results compared with the previously calculated DMC results can be related to the quality of the wave functions and the finite size effects. It has been shown that transition metal PPs that are used in this work yield much improved first and second ionization potentials compared with previous DMC calculations [59]. Therefore, the improved results can be a direct consequence of using better optimized PPs for the excited-state properties.

B. MnO_2

The various calculated quantities (equilibrium volume, bulk modulus, bulk modulus's pressure derivative, and cohesive energies) for MnO_2 using different computational schemes are given in Table II, along with the available computational [33] and experimental results [72,91,92]. For the ground state, we used AFM-I type magnetic configuration since the magnetic and crystallographic space groups are the same. Parallel spins are aligned on the (001) place, whereas an antiparallel orientation exists in [111] direction. Similar to MnO, our DMC-calculated values agree better with the experimental results compared with various DFT functionals. Among all the DFT functionals used in the present work, the bulk modulus and cohesive energies, calculated with PBE, are found to be closest compared with experimental results, while PBEsol predicts the

TABLE I. Excited-state properties of MnO. DFT calculations are differences in Kohn-Sham eigenstates, whereas DMC stands for the optical band gap and DMC_{QP} is the quasiparticle gap.

	Indirect gap (eV)	Direct gap (eV)
DMC	3.74(19)	4.0(2)
	4.47(16) [26], 4.8(2) [63]	
PBE	0.98	1.31
PBE + U	1.12	1.28
SCAN	0.79	1.46
SCAN + U	0.86	1.53
HSE03 [94]	2.6	3.2
HSE03 + G_0W_0 [94]	3.4	4.0
DMC_{QP}	3.98(21), 4.55(26) [26]	
Experiment	3.9(4) [95], 4.0(2) [96], 3.7(1) [97]	

TABLE II. The calculated equilibrium volume, bulk modulus (B), bulk modulus's pressure derivative (B'), and cohesive energies (E^{Coh}) of MnO_2. For comparison, available computational [33] and experimental [35,72,91,92] results are also included. An asterisk (*) denotes results generated in the present work. The statistical uncertainty in DMC is provided in parentheses.

–	Volume/f.u. (Å^3)	B (GPa)	B'	E^{Coh} (eV)
LDA	26.28*	424.65*	5.32*	16.76*
PBE	28.23*, 28.24 [33]	344.77*	5.06*	13.83*
PBEsol	27.20*	387.48*	5.27*	15.33*
Rev PBE	29.03*	310.89*	4.98*	12.36*
PBE + U	29.06*, 29.66 [33]	304.40*	5.55*	11.62*
PBEsol + U	27.99*	349.77*	5.67*	12.53*
PBE0	27.53 [33]			
HSE	27.64 [33]			
DMC	26.59*	289.00*	5.14*	13.54(3)
Exp	27.38 [91], 27.8 [92]	328(18) [91]	4(2) [91]	13.52(2) [72]
	27.74 [35]			

equilibrium volume with the lowest relative error. However, both PBE and PBEsol fail to predict the correct energy ordering of MnO_2 polymorphs [3].

For equilibrium volume, the relative error for PBE+U (5.78%), revised PBE (5.67%), and LDA (4.19%), while the DMC method gives roughly half of the relative error difference (2.97%), and the PBEsol and PBEsol+U methods gives roughly of 0.64% and 2.19%, respectively. Particularly noticeable are the results for calculated cohesive energies, where PBE+U, PBEsol+U, and revised PBE show a tendency to overbind with a relative error of 16.36%, 7.93%, and 9.43%, respectively.

Our DMC-calculated cohesive energy of ground-state structure β-MnO_2 (13.54 ± 0.03 eV) is in excellent agreement with available experimental results (13.52 ± 0.02 eV). We also compare the relative error in calculated equilibrium volume and cohesive energies obtained using different computational schemes as shown in Figs. 5(a) and 5(b).

Hossain *et al.* [98] studied the band gap of β-MnO_2 thin films using conductivity experiments, whereas Li *et al.* [99] performed UV-Vis absorption spectroscopy measurements on β-MnO_2 powders that are prepared using electrodeposition. Our literature search provided no results for optical measurements on the single crystals of β-MnO_2. Sato *et al.* [100] showed that even under highly controlled environments, it is possible to have very small nonstoichiometry β-$MnO_{2-\gamma}$, $\gamma = 0.0014$, in the single crystals. It was shown that even a very small nonstoichiometry in β-MnO_2 can lead to metallic-like properties (e.g., conductive surface states) [100,101]. Since the electronic properties of β-MnO_2 can be very sensitive with respect to defects, it would be misleading to compare the results in Ref. [98] to the bulk β-MnO_2. However, it must be noted that in Ref. [99] the exact crystalline structure of the samples are not reported, but it is shown that two of the x-ray diffraction peaks correspond to the orthorhombic phase. The only orthorhombic phase available to MnO_2 is the Ramsdelite, R-MnO_2, phase. Among all the MnO_2 phases, β-MnO_2 has the smallest known experimental formation energy [92], which is only smaller than the R-MnO_2 phase by 56 ± 32 meV/MnO_2. It is likely that these two phases can coexist at room temperature depending on the technique used to prepare the samples. Therefore, we used the ultraviolet-visible (UV-Vis) absorption spectroscopy measurements of Li *et al.* [99] as the experimental reference for the band gap of β-MnO_2, 2.57 eV, although further experimental studies are needed.

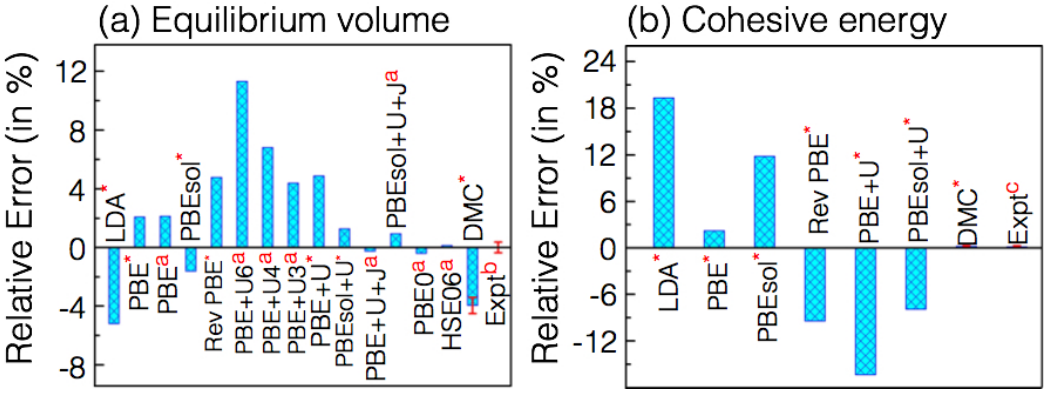

FIG. 5. Comparison (relative error) of calculated and available computational and experimental results for (a) lattice constants and (b) cohesive energies of β-MnO_2. Standard deviation error bars (red bars) show statistical uncertainties in the DMC data. An asterisk (*) denotes results from the present work, while the available results are collected from *a* [33], *b* [35,91,92], and *c* [72].

TABLE III. Excited-state properties of β-MnO_2 calculated at different levels of theory. DFT calculations are differences in Kohn-Sham eigenstates, whereas DMC stands for the optical band gap and DMC_{QP} is the quasiparticle gap. All values are given in eV.

	PBE + U	HSE	SCAN	DMC	DMC_{QP}	Expt.
E_g	0.2 [3]	1.75 [3]	0.43 [3]	2.27(28)	2.19(50)	0.27 [98] 2.57 [99]

In Table III, we presented our results for the excited-state properties of β-MnO_2. Using PBE+U calculations, we determined that β-MnO_2 is a direct band gap material at the Γ point, $E_g^{\Gamma\to\Gamma}$. For β-MnO_2, we performed QP calculations in DMC via two-point extrapolation at 36- and 48-atom cells. We found very good agreement with the experimental band gap of β-MnO_2 and the DMC calculations. We found the DMC quasiparticle and optical gaps to be close to each other; however, the DMC optical gap is the quantity that must be compared against the UV-Vis result in Ref. [99].

C. $LaMnO_3$

Now, we move to the manganese-based ternary oxide namely, $LaMnO_3$. In Figs. 6(a) and 6(b), we compare the relative error (with respect to the experimental values) in calculated lattice parameters and cohesive energies of cubic $LaMnO_3$. In this work we used the 10-atom rhombohedral $LaMnO_3$ unit cell for all calculations [79]. We used the AFM-I magnetic configuration on this unit cell, where the spins on the two cobalt atoms are in antiparallel alignment. In the structural analysis, shown in Fig. 6(a), it is surprising that HF provides the best lattice parameter among all mean field calculations. LDA underestimates the lattice parameter while PBE leads to overestimation, which is typically observed in many materials. Among all the computational approaches compared in the present work, DMC-predicted lattice parameters are in best agreement with available experimental results, followed by HF [105], UHF [104], and B3LYP [102]. In our calculations, the DMC method gives the lowest percent error (0.47%) in lattice parameters, while revPBE gives the highest percent error (1.44%).

TABLE IV. Excited-state properties of LaMnO3 (in eV) DFT calculations are differences in Kohn-Sham eigenstates, whereas DMC_{QP} is the quasiparticle gap. The optical band gap is not calculated at the DMC level because of computational limitations.

	PBE + U	HSE	B3LYP	GW	DMC_{QP}	Expt.
E_g	0.2	2.47 [112]	2.3 [113]	0.82 [114], 0.96 [115], 1.6 [117]	1.45(15)	1.1 [8], 1.3 [116], 1.7 [118]

In the case of cohesive energies, behavior differs considerably among methods, varying up to 9.9% (observed using LDA method). Better DFT cohesive energies were obtained using PBE and PBE+U methods, with only 1.60% and 1.84% deviation. We derived the experimental cohesive energy to be 30.6(5) eV and found that all DFT methods, except revPBE, overbind the atoms in $LaMnO_3$ crystal. The relative error for the revPBE approximation was 2.07%. In comparison, the DMC method provided the best cohesive energy with only a 0.64% error, slightly underbinding the $LaMnO_3$ crystal.

Table IV presents our results for the optical and quasiparticle gaps of $LaMnO_3$. All DFT results presented were obtained from generalized Kohn Sham eigenstates. We present only the quasiparticle gap using DMC for $LaMnO_3$. We performed QP calculations in DMC via a two-point extrapolation using 20- and 40-atom cells. Our PBE + U calculations yield an indirect transition from (0.389,0.0,0.5) to Γ wave vectors. Therefore, the calculation of the optical transition requires a very large supercell. Similarly, all the band structure calculation methods shown in Table IV predict an indirect band gap for $LaMnO_3$. Compared with the rest of the theoretical methods investigated, our DMC results have better agreement with the experiments, although experimental uncertainty is rather large, 1.1–1.7 eV.

IV. CROSS COMPARISON

The most common computational approaches to studying the properties of solids are based on DFT. Despite the application and success of DFT in many branches of science and engineering, however, transition metal-based compounds

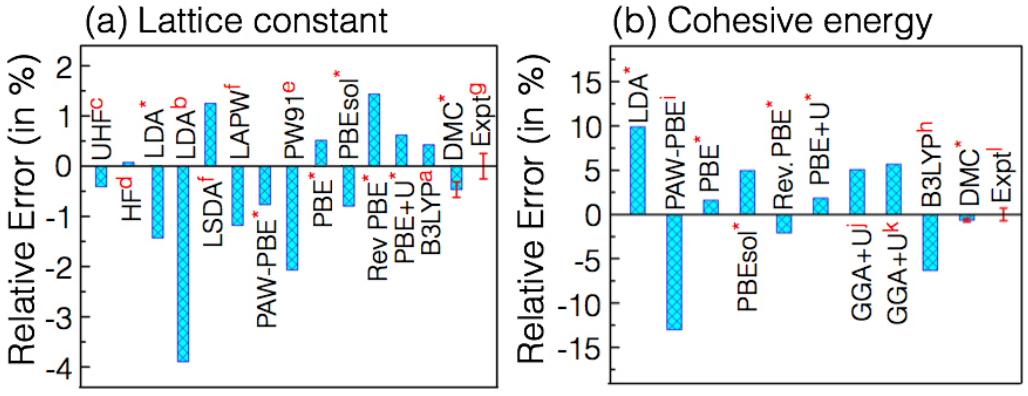

FIG. 6. Comparison (relative error) of calculated and available computational and experimental results for (a) lattice constants and (b) cohesive energies of $LaMnO_3$. Standard deviation error bars (red bars) show statistical uncertainties in the DMC data. An asterisk (*) denotes results from the present work, while the available results are collected from *a* [102], *b* [103], *c* [104], *d* [105], *e* [106], *f*[107], *g* [108], *h* [109], *i* [106], *j* [110], *k* [111], and *l* [76–79].

remain challenging to study using current approximations of DFT [16–29]. This section presents a comparative analysis of various properties of manganese-based oxides calculated from different computational techniques. The aim is to provide a comparative picture of the performance of exchange-correlation functionals in predicting the properties of various manganese-based oxides.

As mentioned earlier, prediction of the correct ground-state structure is one of the most basic properties used to validate the accuracy of any underlying approximation. Most of the semilocal functionals (LDA, PBE, PBEsol, and AM05), Hubbard-corrected (PBE + U [30]), and hybrid functionals (HSE06 [30]) contradict the experimental observation on the prediction of the ground-state structure of MnO [see Fig. 3(a)]. Whereas other than DMC only PW91 [31], revised PBE and random phase approximation (RPA) [30] correctly predicted the RS phase as the ground state of MnO. Although revised PBE correctly identified the ground state of MnO, this is likely fortuitous because it overestimated the lattice parameter by ∼2.5% and underestimated the cohesive energy by ∼25%.

As is evident from Figs. 3(b) and 3(c), the accuracy of semilocal and hybrid functionals in predicting lattice parameters and cohesive energies ranges from 1% to 4%, respectively. Moreover, most semilocal and hybrid functionals also overestimated the bulk modulus for the RS phase of MnO. However, the bulk modulus in the RPA is in good agreement with experimental results irrespective of the considerable variations among different experimental values [69,87–89]. As shown in Figs. 3(a)–3(c), Table V and VI, the present and previously published [26,63] DMC results for lattice parameters, bulk moduli, and cohesive energies lie within the experimental uncertainties.

TABLE VI. DMC-calculated cohesive energies (per f.u.) along with available mean experimental values for MnO [73], MnO_2 [73–75], and $LaMnO_3$ [76–79].

	MnO	MnO_2	$LaMnO_3$
DMC	9.52 (4)	13.54 (3)	30.32 (6)
Expt.	9.50 (2)	13.52 (2)	30.6 (5)

In the case of β-MnO_2, PBE, revised PBE, and most of the Hubbard-corrected functionals overestimate the equilibrium volume, while PBEsol underestimates the volume by ∼2% [Fig. 5(a)]. Figure 5(a) also suggests that the equilibrium volume of MnO_2 increases with the increased value of U in Hubbard-corrected functionals. For $LaMnO_3$, similar to two other cases, semilocal functionals largely underestimate the lattice constant by 1% to 4%. However, Hubbard-corrected and hybrid functionals predict lattice parameters and energetics better and repair the weakness of the semilocal functionals. Basically, for all compounds the accuracy in the lattice parameters and cohesive energies increases as we move from semilocal to hybrid functionals. However, the most accurate results, within the experimental uncertainties, are obtained from DMC. For example, in Table II, we compare the DMC-calculated cohesive energies with the mean experimental values.

To date, materials modeling has been largely dominated by either quantum mechanical methods (e.g., DFT) or force-field–based methods. Both approaches are versatile and have shown potential for providing a good description of a range of chemistries and chemical environments. However, because of the limited predictive power of existing approximate exchange-

TABLE V. The calculated equilibrium lattice parameter (a), bulk modulus (B), bulk modulus's pressure derivative (B'), and cohesive energies (E^{Coh}) of the RS phase of MnO. For comparison, available computational and experimental results are also included. The statistical uncertainty in DMC is provided in parentheses. Fock-0.35 [65] and Fock-0.50 [65] are hybrid functionals with PBE and fraction of HF exchange 0.35 and 0.50, respectively. An asterisk (*) denotes results obtained in the present work.

	a (Å)	B (GPa)	B'	E^{Coh} (eV)
UHF	4.53 [62]			6.20 [62]
HF	4.38 [64]			–
LDA	4.35*, 4.32 [65]	184 [65], 170 [84]		8.08*
GGA (ideal)	4.44 [26]	196	3.9 [84]	9.73 [26]
GGA (relaxed)	4.46 [26]	196 [85]	3.9 [85]	9.74 [26]
PBE	4.37*, [64], 4.45 [65], 4.47 [30]	141*,147 [65], 145 [30]	3.8*	9.20*
PBEsol	4.41*	156*	4.6*	9.00*
Rev. PBE	4.55*	256*	4.30*	7.60*
B3PW91	4.46 [65]	154 [65]		
PBE + U	4.48 [64]			10.77*
LDA + U	4.40 [65]	174 [65]	3.2 [84]	
RPA	4.49 [30]	158 [30]		
Fock-0.35	4.40 [65]	174 [65]		
Fock-0.50	4.44 [65]	170 [65]		
B3LYP	4.50 [64,86]			9.21 [86]
PBE0	4.51 [65], 4.40 [64]	143 [65]		
HSE	4.43 [84]	187 [84]	3.3 [84]	
DMC	4.43 [26]	163 [26]		9.41 [26]
DMC	4.43*	158*	4.1*	9.43 (7)*
Expt.	4.43 [66,67], 4.445 [68–70] 4.446 [69]	144 [69],147 [87],150 [87] 148 [69], 151 [89], 162 [88]	4.8(±1.1) [87,88], 4, 5.28 [69]	9.50 [70–72]

correlation energy functionals, significant failures have been made in predicting the properties of transition metal oxides. Particularly for manganese-based oxides such as $TbMnO_3$ [119,120], $HoMnO_3$ [121], AMn_2O_4 (A = Co and Zn) [122], $CaMn_7O_{12}$ [123], and mixed metal oxides [124], DFT results are very sensitive to the choice of the parameters and/or functionals. Having established the accuracy of the DMC methods in predicting the properties of manganese-based oxides—namely MnO, MnO_2, and $LaMnO_3$—we now have confidence that the DMC methodology is the gold standard to be applied to obtain accurate results in more complex manganese-based oxides.

V. CONCLUSIONS

We have demonstrated the accuracy of the DMC methods in predicting the structural and electronic properties of manganese-based binary (MnO and MnO_2) and ternary ($LaMnO_3$) oxides. Our results for MnO are within the error bars of previous DMC calculations [26,63] performed using different PPs, basis sets, and QMC codes. DMC-calculated lattice constants (except for MnO_2), bulk modulus, and cohesive energies are found to be within the uncertainty of the available experiments. DMC has produced accurate ground and excited-state energies for manganese-based oxides, which exhibit strong electron correlation effects. The present work validates the use of DMC methods for manganese-based oxides, which have complicated electronic structure and are challenging to theory. Having applied DMC to relatively simple polymorphs where good experimental data is available, we have confidence that the methodology can be applied to obtain accurate results in more complex manganese-based oxides such as manganites and manganese-based mixed metal oxides suitable for electrochemical energy storage and conversion devices, catalysis to electronic devices.

ACKNOWLEDGMENTS

K.S., J.T.K., and F.A.R. were supported by the Materials Sciences and Engineering Division of the U.S. Department of Energy, Office of Science, Basic Energy Sciences. P.R.C.K. (DFT and QMC discussions) was supported by the U.S. Department of Energy, Office of Science, Basic Energy Sciences, Materials Sciences and Engineering Division, as part of the Computational Materials Sciences Program and Center for Predictive Simulation of Functional Materials. This research used resources of the Oak Ridge Leadership Computing Facility at Oak Ridge National Laboratory, which is supported by the Office of Science of the U.S. Department of Energy under Contract No. DE-AC05-00OR22725. This manuscript has been authored by UT-Battelle, LLC, under Contract No. DE-AC05-00OR22725 with the U.S. Department of Energy (DOE). The U.S. government retains and the publisher, by accepting the article for publication, acknowledges that the U.S. government retains a nonexclusive, paid-up, irrevocable, worldwide license to publish or reproduce the published form of this manuscript, or allow others to do so, for U.S. government purposes. DOE will provide public access to these results of federally sponsored research in accordance with the DOE Public Access Plan (http://energy.gov/downloads/doe-public-access-plan).

[1] N. Mott, J. Solid State Chem. **88**, 5 (1990).
[2] M. Imada, A. Fujimori, and Y. Tokura, Rev. Mod. Phys. **70**, 1039 (1998).
[3] D. A. Kitchaev, H. Peng, Y. Liu, J. Sun, J. P. Perdew, and G. Ceder, Phys. Rev. B **93**, 045132 (2016).
[4] J. G. Bednorz and K. A. Müller, in *Ten Years of Superconductivity: 1980–1990* (Springer, 1986), pp. 267–271.
[5] R. von Helmolt, J. Wecker, B. Holzapfel, L. Schultz, and K. Samwer, Phys. Rev. Lett. **71**, 2331 (1993).
[6] M. B. Salamon and M. Jaime, Rev. Mod. Phys. **73**, 583 (2001).
[7] K. Wang, J.-M. Liu, and Z. Ren, Adv. Phys. **58**, 321 (2009).
[8] T. Arima, Y. Tokura, and J. B. Torrance, Phys. Rev. B **48**, 17006 (1993).
[9] H. Tanaka and M. Misono, Curr. Opin. Solid State Mater. Sci. **5**, 381 (2001).
[10] J. Suntivich, H. A. Gasteiger, N. Yabuuchi, H. Nakanishi, J. B. Goodenough, and Y. Shao-Horn, Nat. Chem. **3**, 546 (2011).
[11] J. He and C. Franchini, Phys. Rev. B **86**, 235117 (2012).
[12] W. Kohn and L. J. Sham, Phys. Rev. **140**, A1133 (1965).
[13] W. Kohn, Rev. Mod. Phys. **71**, 1253 (1999).
[14] R. M. Martin, *Electronic Structure: Basic Theory and Practical Methods* (Cambridge University Press, Cambridge, 2004).
[15] J. P. Perdew and A. Zunger, Phys. Rev. B **23**, 5048 (1981).
[16] C. Mitra, J. T. Krogel, J. A. Santana, and F. A. Reboredo, J. Chem. Phys. **143**, 164710 (2015).
[17] J. A. Santana, J. T. Krogel, J. Kim, P. R. Kent, and F. A. Reboredo, J. Chem. Phys. **142**, 164705 (2015).
[18] F. Ma, S. Zhang, and H. Krakauer, New J. Phys. **15**, 093017 (2013).
[19] J. Yu, L. K. Wagner, and E. Ertekin, J. Chem. Phys. **143**, 224707 (2015).
[20] G. H. Booth, A. Grüneis, G. Kresse, and A. Alavi, Nature **493**, 365 (2013).
[21] J. A. Santana, J. T. Krogel, P. R. Kent, and F. A. Reboredo, J. Chem. Phys. **144**, 174707 (2016).
[22] D. Alfe and M. J. Gillan, Phys. Rev. B **71**, 220101 (2005).
[23] E. Ertekin, L. K. Wagner, and J. C. Grossman, Phys. Rev. B **87**, 155210 (2013).
[24] H. Zheng and L. K. Wagner, Phys. Rev. Lett. **114**, 176401 (2015).
[25] Y. Luo, A. Benali, L. Shulenburger, J. T. Krogel, O. Heinonen, and P. R. Kent, New J. Phys. **18**, 113049 (2016).
[26] J. A. Schiller, L. K. Wagner, and E. Ertekin, Phys. Rev. B **92**, 235209 (2015).
[27] Y. Lin, R. E. Cohen, S. Stackhouse, K. P. Driver, B. Militzer, L. Shulenburger, and J. Kim, Phys. Rev. B **90**, 184103 (2014).
[28] L. K. Wagner and P. Abbamonte, Phys. Rev. B **90**, 125129 (2014).
[29] K. Foyevtsova, J. T. Krogel, J. Kim, P. R. C. Kent, E. Dagotto, and F. A. Reboredo, Phys. Rev. X **4**, 031003 (2014).

[30] H. Peng and S. Lany, Phys. Rev. B **87**, 174113 (2013).
[31] A. Schrön, C. Rödl, and F. Bechstedt, Phys. Rev. B **82**, 165109 (2010).
[32] E. Cockayne, I. Levin, H. Wu, and A. Llobet, Phys. Rev. B **87**, 184413 (2013).
[33] C. Franchini, R. Podloucky, J. Paier, M. Marsman, and G. Kresse, Phys. Rev. B **75**, 195128 (2007).
[34] L. K. Wagner, M. Bajdich, and L. Mitas, J. Comput. Phys. **228**, 3390 (2009).
[35] N. Ohama and Y. Hamaguchi, J. Phys. Soc. Jpn. **30**, 1311 (1971).
[36] J. Kim, K. P. Esler, J. McMinis, M. A. Morales, B. K. Clark, L. Shulenburger, and D. M. Ceperley, J. Phys.: Conf. Ser. **402**, 012008 (2012).
[37] K. Esler, J. Kim, D. Ceperley, and L. Shulenburger, Comput. Sci. Eng. **14**, 40 (2012).
[38] L. K. Wagner and D. M. Ceperley, Rep. Prog. Phys. **79**, 094501 (2016).
[39] R. Q. Hood, P. R. C. Kent, and F. A. Reboredo, Phys. Rev. B **85**, 134109 (2012).
[40] W.-K. Leung, R. J. Needs, G. Rajagopal, S. Itoh, and S. Ihara, Phys. Rev. Lett. **83**, 2351 (1999).
[41] E. Ertekin, M. T. Winkler, D. Recht, A. J. Said, M. J. Aziz, T. Buonassisi, and J. C. Grossman, Phys. Rev. Lett. **108**, 026401 (2012).
[42] R. Q. Hood, P. R. C. Kent, R. J. Needs, and P. R. Briddon, Phys. Rev. Lett. **91**, 076403 (2003).
[43] N. Devaux, M. Casula, F. Decremps, and S. Sorella, Phys. Rev. B **91**, 081101 (2015).
[44] K. P. Esler, R. E. Cohen, B. Militzer, J. Kim, R. J. Needs, and M. D. Towler, Phys. Rev. Lett. **104**, 185702 (2010).
[45] J. A. Santana, J. T. Krogel, P. R. C. Kent, and F. A. Reboredo, J. Chem. Phys. **147**, 034701 (2017).
[46] J. T. Krogel, Comput. Phys. Commun. **198**, 154 (2016).
[47] B. M. Austin, D. Y. Zubarev, and W. A. Lester Jr, Chem. Rev. **112**, 263 (2011).
[48] L. K. Wagner, Int. J. Quant. Chem. **114**, 94 (2014).
[49] L. Shulenburger and T. R. Mattsson, Phys. Rev. B **88**, 245117 (2013).
[50] W. Foulkes, L. Mitas, R. Needs, and G. Rajagopal, Rev. Mod. Phys. **73**, 33 (2001).
[51] C. Lin, F. H. Zong, and D. M. Ceperley, Phys. Rev. E **64**, 016702 (2001).
[52] J. C. Slater, Phys. Rev. **81**, 385 (1951).
[53] V. Fock, Z. Physik **61**, 126 (1930).
[54] R. Jastrow, Phys. Rev. **98**, 1479 (1955).
[55] J. Toulouse and C. J. Umrigar, J. Chem. Phys. **126**, 084102 (2007).
[56] P. Giannozzi, S. Baroni, N. Bonini, M. Calandra, R. Car, C. Cavazzoni, D. Ceresoli, G. L. Chiarotti, M. Cococcioni, I. Dabo, A. Dal Corso, S. de Gironcoli, S. Fabris, G. Fratesi, R. Gebauer, U. Gerstmann, C. Gougoussis, A. Kokalj, M. Lazzeri, L. Martin-Samos, N. Marzari, F. Mauri, R. Mazzarello, S. Paolini, A. Pasquarello, L. Paulatto, C. Sbraccia, S. Scandolo, G. Sclauzero, A. P. Seitsonen, A. Smogunov, P. Umari, and R. M. Wentzcovitch, J. Phys.: Condens. Matter **21**, 395502 (2009).
[57] G. Kresse and J. Furthmüller, Phys. Rev. B **54**, 11169 (1996).
[58] G. Kresse and J. Furthmüller, Comput. Mater. Sci. **6**, 15 (1996).
[59] J. T. Krogel, J. A. Santana, and F. A. Reboredo, Phys. Rev. B **93**, 075143 (2016).
[60] A. L. Dzubak, J. T. Krogel, and F. A. Reboredo, J. Chem. Phys. **147**, 024102 (2017).
[61] M. Casula, Phys. Rev. B **74**, 161102 (2006).
[62] M. D. Towler, N. L. Allan, N. M. Harrison, V. R. Saunders, W. C. Mackrodt, and E. Aprà, Phys. Rev. B **50**, 5041 (1994).
[63] L. Mitas and J. Kolorenč, Rev. Mineral. Geochem. **71**, 137 (2010).
[64] C. Franchini, V. Bayer, R. Podloucky, J. Paier, and G. Kresse, Phys. Rev. B **72**, 045132 (2005).
[65] F. Tran, P. Blaha, K. Schwarz, and P. Novák, Phys. Rev. B **74**, 155108 (2006).
[66] W. Roth, Phys. Rev. **110**, 1333 (1958).
[67] B. Fender, A. Jacobson, and F. Wedgwood, J. Chem. Phys. **48**, 990 (1968).
[68] R. W. G. Wyckoff and R. W. Wyckoff, *Crystal Structures*, Vol. 2 (Interscience, New York, 1960).
[69] J. Zhang, Phys. Chem. Miner. **26**, 644 (1999).
[70] Y. Sumino, M. Kumazawa, O. Nishizawa, and W. Pluschkell, J. Phys. Earth **28**, 475 (1980).
[71] I. Barin and G. Platzki, *Thermochemical Data of Pure Substances*, Vol. 304 (VCH Publishers Inc., New York, NY, 1989).
[72] H. Schlosser, Phys. Status Solidi (b) **179**, K1 (1993).
[73] W. A. Harrison, Phys. Rev. B **77**, 245103 (2008).
[74] M. Zhuang and J. W. Halley, Phys. Rev. B **64**, 024413 (2001).
[75] W. Harrison, *Elementary Electronic Structure* (World Scientific Publishing, Singapore, 1999).
[76] M. W. Chase, *Journal of Physical and Chemical Reference Data*, Monograph No. 9 (AIP, New York, 1998).
[77] G. Sinquin, C. Petit, J. Hindermann, and A. Kiennemann, Catal. Today **70**, 183 (2001).
[78] L. Rørmark, S. Stølen, K. Wiik, and T. Grande, J. Solid State Chem. **163**, 186 (2002).
[79] J. Rodriguez-Carvajal, M. Hennion, F. Moussa, A. H. Moudden, L. Pinsard, and A. Revcolevschi, Phys. Rev. B **57**, R3189 (1998).
[80] F. Murnaghan, Proc. Natl. Acad. Sci. USA **30**, 244 (1944).
[81] R. J. Needs, P. R. C. Kent, A. R. Porter, M. D. Towler, G. Rajagopal, T. C. M. Group, M. Road, C. Cb, and U. Kingdom, Int. J. Quant. Chem. **86**, 218 (2002).
[82] A. J. Williamson, R. Q. Hood, R. J. Needs, and G. Rajagopal, Phys. Rev. B **57**, 12140 (1998).
[83] V. I. Anisimov, F. Aryasetiawan, and A. I. Lichtenstein, J. Phys. Condens. Matter **9**, 767 (1997).
[84] D. Kasinathan, J. Kuneš, K. Koepernik, C. V. Diaconu, R. L. Martin, I. D. Prodan, G. E. Scuseria, N. Spaldin, L. Petit, T. C. Schulthess, and W. E. Pickett, Phys. Rev. B **74**, 195110 (2006).
[85] R. E. Cohen, I. Mazin, and D. G. Isaak, Science **275**, 654 (1997).
[86] X. Feng, Phys. Rev. B **69**, 155107 (2004).
[87] R. Pacalo and E. Graham, Phys. Chem. Miner. **18**, 69 (1991).
[88] R. Jeanloz and A. Rudy, J. Geophys. Res.: Solid Earth **92**, 11433 (1987).
[89] Y. Noguchi, K. Kusaba, K. Fukuoka, and Y. Syono, Geophys. Res. Lett. **23**, 1469 (1996).
[90] C. G. Shull, W. A. Strauber, and E. O. Wollan, Phys. Rev **83**, 333 (1951).
[91] J. Haines, J. Léger, and S. Hoyau, J. Phys. Chem. Solids **56**, 965 (1995).

[92] S. Fritsch, J. E. Post, S. L. Suib, and A. Navrotsky, Chem. Mater. **10**, 474 (1998).
[93] L. He, F. Liu, G. Hautier, M. J. T. Oliveira, M. A. L. Marques, F. D. Vila, J. J. Rehr, G. M. Rignanese, and A. Zhou, Phys. Rev. B **89**, 064305 (2014).
[94] C. Rodl, F. Fuchs, J. Furthmuller, and F. Bechstedt, Phys. Rev. B Condens. Matter Mater. Phys. **79**, 235114 (2009).
[95] J. van Elp, J. L. Wieland, H. Eskes, P. Kuiper, G. A. Sawatzky, F. M. F. de Groot, and T. S. Turner, Phys. Rev. B **44**, 6090 (1991).
[96] I. A. Drabkin, L. T. Emelyanova, R. N. Iskenderov, and Y. M. Ksendzov, Fiz. Tverd. Tela **10**, 3082 (1968).
[97] I. A. Drabkin and Y. M. Ksendzov, Fiz. Tverd. Tela **7**, 1884 (1965).
[98] M. S. Hossain, R. Islam, M. Shahjahan, and K. A. Khan, J. Mater. Sci.: Mater. Electron. **19**, 1114 (2008).
[99] T. Li, J. Wu, X. Xiao, B. Zhang, Z. Hu, J. Zhou, P. Yang, X. Chen, B. Wang, and L. Huang, RSC Adv. **6**, 13914 (2016).
[100] H. Sato, T. Enoki, M. Isobe, and Y. Ueda, Phys. Rev. B **61**, 3563 (2000).
[101] D. A. Tompsett and M. S. Islam, J. Phys. Chem. C **118**, 25009 (2014).
[102] D. Fuks, L. Bakaleinikov, E. Kotomin, J. Felsteiner, A. Gordon, R. Evarestov, D. Gryaznov, and J. Maier, Solid State Ionics **177**, 217 (2006).
[103] G. Pilania and R. Ramprasad, Surf. Sci. **604**, 1889 (2010).
[104] M. Nicastro and C. H. Patterson, Phys. Rev. B **65**, 205111 (2002).
[105] R. Evarestov, E. Kotomin, E. Heifets, J. Maier, and G. Borstel, Solid State Commun. **127**, 367 (2003).
[106] E. Kotomin, R. Evarestov, Y. A. Mastrikov, and J. Maier, Phys. Chem. Chem. Phys. **7**, 2346 (2005).
[107] D. Fuks, S. Dorfman, J. Felsteiner, L. Bakaleinikov, A. Gordon, and E. Kotomin, Solid State Ionics **173**, 107 (2004).
[108] C. Raisch, C. Langheinrich, R. Werner, R. Kleiner, D. Koelle, M. Glaser, T. Chassé, and A. Chassé, J. Appl. Phys. **113**, 063511 (2013).
[109] E. A. Ahmad, L. Liborio, D. Kramer, G. Mallia, A. R. Kucernak, and N. M. Harrison, Phys. Rev. B **84**, 085137 (2011).
[110] S. Piskunov, E. Heifets, T. Jacob, E. A. Kotomin, D. E. Ellis, and E. Spohr, Phys. Rev. B **78**, 121406 (2008).
[111] E. A. Kotomin, Y. A. Mastrikov, E. Heifets, and J. Maier, Phys. Chem. Chem. Phys. **10**, 4644 (2008).
[112] J. He, M.-X. Chen, X.-Q. Chen, and C. Franchini, Phys. Rev. B **85**, 195135 (2012).
[113] D. Muñoz, N. M. Harrison, and F. Illas, Phys. Rev. B **69**, 085115 (2004).
[114] Y. Nohara, A. Yamasaki, S. Kobayashi, and T. Fujiwara, Phys. Rev. B **74**, 064417 (2006).
[115] Z. Ergonenc, B. Kim, P. Liu, G. Kresse, and C. Franchini, Phys. Rev. Materials **2**, 024601 (2018).
[116] A. Chainani, M. Mathew, and D. D. Sarma, Phys. Rev. B **47**, 15397 (1993).
[117] Y. Nohara, S. Yamamoto, and T. Fujiwara, Phys. Rev. B **79**, 195110 (2009).
[118] T. Saitoh, A. E. Bocquet, T. Mizokawa, H. Namatame, A. Fujimori, M. Abbate, Y. Takeda, and M. Takano, Phys. Rev. B **51**, 13942 (1995).
[119] V. Sharma, A. McDannald, M. Staruch, R. Ramprasad, and M. Jain, Appl. Phys. Lett. **107**, 012901 (2015).
[120] M. Staruch, V. Sharma, C. dela Cruz, R. Ramprasad, and M. Jain, J. Appl. Phys. **116**, 033919 (2014).
[121] S. Picozzi, K. Yamauchi, B. Sanyal, I. A. Sergienko, and E. Dagotto, Phys. Rev. Lett. **99**, 227201 (2007).
[122] Y. Deng, L. Wan, Y. Xie, X. Qin, and G. Chen, RSC Adv. **4**, 23914 (2014).
[123] X. Z. Lu, M.-H. Whangbo, S. Dong, X. G. Gong, and H. J. Xiang, Phys. Rev. Lett. **108**, 187204 (2012).
[124] Y. Guo, L. Yu, C.-Y. Wang, Z. Lin, and X. W. D. Lou, Adv. Funct. Mater. **25**, 5184 (2015).